Natural Frequencies of Submerged Structures Using an Efficient Calculation of the Added Mass Matrix in the Boundary Element Method

Article *in* Journal of vibration and acoustics · September 2018

DOI: 10.1115/1.4041617

CITATIONS
0

READS
74

2 authors:

Luis Monterrubio
Robert Morris University
29 PUBLICATIONS **129** CITATIONS

SEE PROFILE

Petr Krysl
University of California, San Diego
130 PUBLICATIONS **5,540** CITATIONS

SEE PROFILE

Natural Frequencies of Submerged Structures Using an Efficient Calculation of the Added Mass Matrix in the Boundary Element Method

Luis E. Monterrubio[1]
Engineering Department,
Robert Morris University,
6001 University Boulevard,
Moon, PA 15108
e-mail: monterrubio@rmu.edu

Petr Krysl
Structural Engineering Department,
University of California, San Diego,
9500 Gilman Dr., #0085,
La Jolla, CA 92093
e-mail: pkrysl@ucsd.edu

This work presents an efficient way to calculate the added mass matrix, which allows solving for natural frequencies and modes of solids vibrating in an inviscid and infinite fluid. The finite element method (FEM) is used to compute the vibration spectrum of a dry structure, then the boundary element method (BEM) is applied to compute the pressure modes needed to determine the added mass matrix that represents the fluid. The BEM requires numerical integration which results in a large computational cost. In this work, a reduction of the computational cost was achieved by computing the values of the pressure modes with the required numerical integration using a coarse BEM mesh, and then, interpolation was used to compute the pressure modes at the nodes of a fine FEM mesh. The added mass matrix was then computed and added to the original mass matrix of the generalized eigenvalue problem to determine the wetted natural frequencies. Computational cost was minimized using a reduced eigenvalue problem of size equal to the requested number of natural frequencies. The results show that the error of the natural frequencies using the procedure in this work is between 2% and 5% with 87% reduction of the computational time. The motivation of this work is to study the vibration of marine mammals' ear bones. [DOI: 10.1115/1.4041617]

1 Introduction

The natural frequencies and modes of vibration of a structure are usually obtained from the solution of an eigenproblem involving the mass and stiffness matrices of the structure. In some approaches, extra terms are added to the mass matrix to obtain the natural frequencies of a structure submerged in fluid. These terms are called the "added mass" matrix, which account for inertia changes at low frequencies associated with the motion of the fluid caused by the body acceleration of the structure. Similar definitions of "added mass" can be found in the literature as in the work by Lin and Liao [1] and by Gassemi and Yari [2].

Several publications have defined different ways to obtain the added mass matrix or alternatively coupling matrices to solve fluid-structure interaction problems [1–12]. Three interesting procedures to compute the added mass matrix are described in the work by Geers [3], Deruntz and Geers [4], and Antoniadis and Kanarachos [5]. Geers [3] used doubly asymptotic approximations to obtain the acoustic response of the structure. Doubly asymptotic approximations are differential equations for boundary element analysis used to solve fluid-structure interaction and their formulation is based on the representation of the motion of the surface as a linear combination of orthogonal fluid boundary modes. This procedure avoids the use of the boundary element method (BEM), reducing the cost of the analysis. Another advantage of the method is that it is asymptotically exact for low and high frequencies. In the work by Deruntz and Geers [4], a two-dimensional mesh is built on the wet surface of the structure as a first step, and in the second step, a discrete boundary integral method (BIM) is implemented for the treatment of fluid-structure interaction effects. The method in Ref. [4] gives the added mass matrix directly from the matrices obtained in the discrete BIM, provided the velocity of the structure and the fluid are considered to be equal and have common nodes. Antoniadis and Kanarachos [5] presented a general methodology to decouple the structure and fluid domains for modal analysis. They used the common procedure based on the implementation of the finite element method (FEM) to compute the basis vectors of the structure and the corresponding mass and stiffness matrix terms of the dry structure, while the BIM is used to solve a set of potential (Laplacian) problems for the fluid that gives the basis vectors of the fluid pressure also called pressure modes. In Antoniadis and Kanarachos approach [5], each term of the added mass matrix is a function of the modes of vibration of the dry structure, the pressure modes, the normal vector of the boundary element, and the density of the fluid. In addition, Antoniadis and Kanarachos used general coordinate transformations to simplify the expression of the stiffness and mass matrices of the structure. Furthermore, Antoniadis and Kanarachos reported that the FEM can be used instead of the BIM, which is the procedure used by Rajasankar et al. [8] and more recent publications use the fast multipole boundary element method such as Refs. [1,12].

In vibro-acoustic analysis using the FEM, it is necessary to include a large amount of degrees-of-freedom (DOF) in the structure to obtain accurate results. For instance, Jensen et al. [13] recommend using at least 10 elements per wavelength. In addition, it is often required to compute the response of a structure for stimuli at different frequencies. However, using a large number of elements to discretize the structure means that the number of unknowns corresponding to the discretization of the surface for the BEM could also be very large. The BEM simulation unfortunately scales poorly with respect to the number of unknowns as the coefficient matrix is fully populated. Thus, a method to reduce the cost of the BEM simulations is highly desirable.

This work uses the procedure by Antoniadis and Kanarachos with the difference that the pressure modes are first obtained on a coarse BEM mesh, and then, the pressure mode values on a finer

[1]Corresponding author.

Contributed by the Technical Committee on Vibration and Sound of ASME for publication in the Journal of Vibration and Acoustics. Manuscript received August 28, 2017; final manuscript received September 26, 2018; published online November 13, 2018. Assoc. Editor: Stefano Lenci.

BEM mesh are obtained by linear interpolation. It is important to keep in mind that the motivation of this work is to solve for natural frequencies of marine mammals' ear bones from which models are produced using a computed tomography scanner. The resolution of models built by cubic voxels obtained from computed tomography scanners is very fine. For these reasons when working with marine mammal's ear bones models, it was necessary to reduce the size and to smooth the surface of the model with triangular plate elements. For this reason, it was not necessary to implement routines for curved boundary elements. Another advantage of this approach is that it allows to compute the natural frequencies of unconstrained submerged structures without spurious modes. This is a very relevant characteristic of the method, because ear bones of many marine mammals are not attached to the skull. In this work, an ear bone of a marine mammal is modeled as an unconstrained structure.

Although damping can also influence the frequencies and modes of the submerged structure, the effects of structural damping are not taken into account in this work. Excitation of the structure by intermodal coupling is also not taken into account.

A previous conference paper by Monterrubio and Krysl [14] presents a "pilot project" of this work presenting the results of (a) a cantilever plate and (b) an unconstrained plate, while the current paper includes the procedure and results of (a) two different plates, (b) two different unconstrained cylinders, and (c) a marine mammal's ear-bone.

2 Theoretical Derivations

The main purpose of this work is to reduce the computational cost of the pressure modes' calculations to obtain the natural frequencies of submerged structures of complex geometry such as marine mammals' ear bones.

In the first step, the FEM is used with an appropriately fine mesh to obtain the mass and stiffness matrices, and subsequently, the natural frequencies and the modes of the dry structure. In the second step, the pressure modes, due to the interaction of the structure with a fluid, are computed using the BEM using a coarse mesh. The location of the nodes of the coarse mesh coincides with the location of some of the nodes of the fine mesh; this allows to compute the pressure modes on the fine mesh using linear interpolation. Then, the added mass matrix is computed and included in the generalized eigenvalue problem which results in giving the wetted-structure natural frequencies. Thus, the present work follows the procedure given by Antoniadis and Kanarachos [5], but speeds up the computation of the pressure modes eliminating a good number of the numerical integrations necessary in the BEM to obtain the pressure modes.

The procedure in Antoniadis and Kanarachos [5] showed that the vibration problem of a submerged structure can be decoupled into two main subproblems as follows:

Step 1: Compute the mass and stiffness matrices and solve the free-vibration problem of the dry structure using the FEM

$$\mathbf{Kc} - \omega^2 \mathbf{Mc} = \mathbf{0} \tag{1}$$

where $\mathbf{K}$ is the stiffness matrix, $\mathbf{M}$ is the mass matrix, ω is the circular frequency, and $\mathbf{c}$ is a vector of unknown coefficients. The solution of the generalized eigenproblem in Eq. (1) gives the natural frequencies ω_i of the structure and the matrix $\mathbf{\Psi}$ in which columns $\boldsymbol{\psi}_i$ are the corresponding ith orthogonal eigenvectors that define the modes of vibration.

Then, the matrix $\mathbf{\Psi}$ and its transpose $\mathbf{\Psi}^{\mathrm{T}}$ are used to diagonalize the stiffness and mass matrices, provided the eigenvectors are $\mathbf{M}$-orthonormal

$$\mathbf{\Psi}^{\mathrm{T}} \mathbf{K} \mathbf{\Psi} = \Omega^2 \tag{2}$$

$$\mathbf{\Psi}^{\mathrm{T}} \mathbf{M} \mathbf{\Psi} = \mathbf{I} \tag{3}$$

where Ω^2 is a diagonal matrix containing the eigenvalues of Eq. (1) in which square roots are the circular natural frequencies ω_i of the structure and $\mathbf{I}$ is the identity matrix. In the work by Antoniadis and Kanarachos [5], the stiffness, mass, and added mass matrices are normalized in such a way that the stiffness matrix becomes an identity matrix. Following this normalization, m_{ii} terms of the diagonal mass matrix are equal to the inverse of the ith eigenvalues and the terms m^*_{ij} of the added mass terms are divided by the square root of the product of the ith and jth eigenvalues. This step (normalization) is skipped in the present work.

Step 2: Solve the Laplacian problems with the BEM for the fluid using the dry eigenvectors to obtain the pressure modes.

The potential (Laplacian) problem as defined in Ref. [5] is written for an inviscid fluid domain as

$$\Delta P = 0 \tag{4}$$

where P is the modal amplitude of the fluid pressure. The structure coupling effect at the common fluid-structure surface is

$$\partial p / \partial n = \omega^2 \rho_{\mathrm{F}} \mathbf{U} \cdot \mathbf{n} \tag{5}$$

where $\partial p / \partial n$ is the normal derivative of the pressure, ρ_{F} is the density of the fluid, $\mathbf{U}$ is the modal amplitude of the structural displacements, and $\mathbf{n}$ is the unit normal toward the exterior of the solid domain.

The solution of the Laplace equations is obtained using the BEM with N flat boundary elements E_{i} to discretize the surface of the structure D, together with the point collocation technique as described in the work by Pozrikidis [15]. To compute the function f, which are the basis vectors of the fluid pressure also called pressure modes, the following discretized integral equation is applied to the centroid of each boundary element, denoted by $\mathbf{x}_j^M$, where $j = 1, \ldots N$:

$$f\left(\mathbf{x}_j^M\right) = -2 \sum_{i=1}^{N} \left(\frac{\partial f}{\partial n}\right)_i \int_{E_i} G\left(\mathbf{x}, \mathbf{x}_j^M\right) dS(\mathbf{x}) + 2 \sum_{i=1}^{N} f_i \int_{E_i}^{\mathrm{PV}} \left[\mathbf{n}(\mathbf{x}) \cdot \nabla G\left(\mathbf{x}, \mathbf{x}_j^M\right)\right] dS(\mathbf{x}) \tag{6}$$

where $\mathbf{x}$ is a vector defining the location of the variable "field point," $\mathbf{x}_0$ is the fixed location of the "singular point," and G is the free-space Green's function in three dimensions for the Laplace equation

$$G(\mathbf{x}, \mathbf{x}_0) = \frac{1}{4\pi r} \tag{7}$$

where $r = |\mathbf{x} - \mathbf{x}_0|$.

The integrals of the terms on the right-hand side of Eq. (6) are called the single-layer and double-layer integrals, respectively. Setting $f(\mathbf{x}_j^M) = f_j, f_i = \delta_{ij} f_j$ and rearranging

$$\left(A_{ij} - \frac{1}{2}\delta_{ij}\right) f_i = B_{ij} \left(\frac{\partial f}{\partial n}\right)_i \tag{8}$$

where δ_{ij} is Kronecker's delta, and the coefficient matrices A_{ij} and B_{ij} are

$$A_{ij} \equiv \int_{E_i}^{\mathrm{PV}} [\mathbf{n}(\mathbf{x}) \cdot \nabla G(\mathbf{x}, \mathbf{x}_j^M)] dS(\mathbf{x}) \tag{9}$$

$$B_{ij} \equiv \int_{E_i} G(\mathbf{x}, \mathbf{x}_j^M) dS(\mathbf{x}) \tag{10}$$

where PV denotes the principal-value integral, which applies only to the elements that share the evaluation point $\mathbf{x}_0$.

The source strength of the potential is assumed to be uniform in each panel. The coefficients of A_{ij} exhibit a singularity $1/r$, while

the coefficients of B_{ij} exhibit a singularity of $1/r^3$ which are characteristic of Green's functions of Laplace's equation in three dimensions. Thus, it is necessary to rely on numerical integration to evaluate the coefficients A_{ij} and B_{ij} in Eqs. (9) and (10).

For a flat element, $\nabla G(\mathbf{x}, \mathbf{x}_j^M) = 0$, because the normal $\mathbf{n}(\mathbf{x})$ and the vector $|\mathbf{x} - \mathbf{x}_0|$ are perpendicular, thus

$$\nabla G\left(\mathbf{x}, \mathbf{x}_j^M\right) = \mathbf{n}(\mathbf{x}) \cdot (\mathbf{x} - \mathbf{x}_0) \frac{1}{4\pi r^3} = 0 \tag{11}$$

This reduces the computational cost, because the coefficients of A_{ij} for flat boundary elements have zero elements for $i = j$. Furthermore, when solving for natural frequencies of plates, all A_{ij} elements are zero as all elements lie on the same plane.

In this work, the results for submerged plates, cylinders, and an ear-bone are presented. Hexahedral and tetrahedral elements are used to discretize the solid domain, while quadrilateral boundary elements are used to discretize the surface of plates and triangular boundary elements are used to discretize the surface of cylinders and an ear bone in the BEM.

The following schemes were selected to perform the integrals of the single layer and double layers:

(a) for quadrilateral boundary elements used in plates

$$A_{ij} = \begin{cases} 0 & i = j \\ w\nabla G \det \mathbf{J} & i \neq j \end{cases} \tag{12a}$$

where $\det \mathbf{J}$ is the determinant of the Jacobian and

$$B_{ij} = \begin{cases} 7.050989 wG \det \mathbf{J} & i = j \\ wG \det \mathbf{J} & i \neq j \end{cases} \tag{13a}$$

The integration schemes applied to A_{ij} and B_{ij} for $i \neq j$ correspond to the Gauss–Legendre quadrature in two dimensions [16] and one point of integration was used to reduce the computational cost. The integration scheme applied to B_{ij} for $i = j$ was performed according to the numerical integration given by Kwak [9] using two integration points.

(b) for triangular boundary elements used in cylinders and an ear-bone in this work

$$A_{ij} = \begin{cases} 0 & i = j \\ w\nabla G \det \mathbf{J}/2 & i \neq j \end{cases} \tag{12b}$$

$$B_{ij} = \begin{cases} 7.050989 wG^{TV3} \det \mathbf{J}/2 & i = j \\ wG \det \mathbf{J}/2 & i \neq j \end{cases} \tag{13b}$$

where G^{TV3} is the integration scheme with the singularity defined at the origin of the rectangular triangle as given in the work by Pina et al. [17]. This integration scheme uses four integration points at (0.16385498, 0.04756957; 0.61114253, 0.17753138; 0.04756957, 0.16385498; 0.17753138, 0.61114253) with weights 0.31161231, 0.31161293, 0.31161231, and 0.31161293.

After computing the coefficients A_{ij} and B_{ij}, it is possible to solve the Laplace problem, which gives a function f that corresponds to the pressure modes of the structure evaluated at the center of selected elements. The values of the pressure modes at the BEM nodes are obtained by equally distributing the value of the pressure mode computed for the element on the nodes in the case of rectangular boundary elements or linear interpolation when triangular boundary elements are used. Then, linear interpolation is used to compute the pressure modes at the surface nodes of the finer original finite element mesh.

After this, it is possible to compute the terms of the added mass matrix $\mathbf{M}^*$ as follows:

$$M_{ij}^* = \int_D \rho_F \boldsymbol{\psi}_i \cdot f_j \mathbf{n} dD \tag{14}$$

and the natural frequencies of the wet structure are obtained solving the generalized eigenproblem

$$\boldsymbol{\Omega}^2 \mathbf{a} - \omega^2 (\mathbf{I} + \mathbf{M}^*) \mathbf{a} = 0 \tag{15}$$

The above equation is the reduced eigenvalue problem where matrices are of size $n \times n$, where n is the number of requested natural frequencies kept to 5 for plates, 24 for cylinders (due to repeated modes), and 10 for the earbone. This equation is obtained substituting Eqs. (2) and (3) in Eq. (1) and adding the added mass matrix to the mass matrix of the "dry" structure; $\mathbf{a}$ is a vector of unknown coefficients and $\mathbf{I}$ is a unit matrix, while the wet modes of vibration are obtained multiplying the eigenvectors of Eqs. (1) and (15) [18].

2.1 Summary of the Procedure

(i) Create a fine and a coarse finite element mesh. It is recommended that the nodes of the coarse mesh coincide with the location of nodes of the fine mesh.
(ii) Solve the generalized eigenvalue problem in Eq. (1) using the fine mesh to obtain the dry natural frequencies and modes of vibration.
(iii) Inherit "dry modes values" from the nodes in the fine mesh to the coinciding nodes in the coarse mesh.
(iv) Diagonalize the stiffness and mass matrices using Eqs. (2) and (3).
(v) Use the coarse finite element mesh to create the boundary element mesh.
(vi) Using the (coarse) boundary mesh and the dry modes results of the coarse mesh obtains the terms A_{ij} and B_{ij} as defined in Eqs. (9) and (10) using numerical integrations (12) and (13), respectively.
(vii) Solve for pressure modes f in Eq. (8). Note that pressure modes are assigned to the center of the elements.
(viii) Compute the pressure modes in the fine mesh using interpolation.
(ix) Compute the terms of the added mass matrix M_{ij}^* as indicated in Eq. (14). This step also requires computing the normal of each element.
(x) Solve the "wet" generalized eigenvalue problem defined in Eq. (15).

3 Examples

The solution of the dry natural frequencies and wet natural frequencies and modes of vibration of the following structures are presented below:

(a) Unconstrained rectangular plate as presented by Sundqvist [19];
(b) cantilever square plate as presented by Fu and Price [11] and Lindholm et al. [20];
(c) unconstrained cylinder as presented by Price et al [21] and Randall [22];
(d) unconstrained cylinder as presented by Everstine [10] and Gilroy [23];
(e) unconstrained ear-bone of a marine mammal—wet modes are omitted.

The results using the present procedure were obtained using the free software FAESOR by Krysl [24].

The relative error of the solution and the time reduction using interpolation provided in the appropriate sections are defined as

$$\text{error} = 100\% \frac{(\text{results using coarse mesh} - \text{results using fine BEM mesh})}{\text{results using fine BEM mesh}} \tag{16}$$

and

$$\text{time reduction} = 100\%\left(1 - \frac{\text{time using coarse mesh}}{\text{time using fine BEM mesh}}\right) \quad (17)$$

3.1 Unconstrained Rectangular Plate. This example shows the results of the natural frequencies and modes of vibration of an unconstrained rectangular plate submerged in water. The plate has dimensions $a = 0.27$ m and $b = 0.1495$ m along directions x and y, thickness $h = 0.00896$ m, while the material properties are Poisson's ratio $\nu = 0.3$, density $\rho_p = 7797\,\text{kg/m}^3$, and Young's modulus $E = 208.8\,\text{GPa}$. The density of the water was taken as $\rho_w = 997\,\text{kg/m}^3$.

In this section, the results of the natural frequencies and modes of vibration of the plate were obtained using the 20-node serendipity hexahedron H20 element in the finite element code FAESOR. Table 1 shows the results of the dry frequencies obtained experimentally, using the FEM code ADINA presented by Sundqvist [19], a set of results using FAESOR and using the Rayleigh–Ritz method [25]. The results using the present approach (FAESOR) correspond to a model with 24 elements along the sides aligned in the x and y directions and 1 element across the thickness. The results in the publication by Sundqvist [19] were obtained from four models of a quarter of the plate (each with 3947 DOF) with different combinations of symmetrical and antisymmetrical boundary conditions. The results for the first eleven modes of the unconstrained plate were computed, but the results of the first six rigid body modes are not included in Table 1.

The results of the natural frequencies of the unconstrained plate submerged in water are presented in Table 2. The results obtained in FAESOR are compared to experimental results and FEM (ADINA) results presented by Sundqvist [19]. The first set of results using the procedure described in this work corresponds to the model presented in Table 1 computing the pressure modes at all elements. The last three columns in Table 2 present the results obtained computing the pressure modes using coarser BEM meshes. These meshes have $12 \times 12 = 144$, $8 \times 8 = 64$, and $6 \times 6 = 36$ identical elements. The DOF included in these boundary element models can be calculated multiplying the number of nodes in the mesh by three, because only translational DOFs are used to calculate the pressure modes at the center of each element. Then, the pressure modes at the nodes of the boundary elements that coincide with the surface of the finite element mesh are obtained by linear interpolation. Figure 1 shows the original 24×24 finite element mesh (left) and the 6×6 boundary element mesh (right) used to compute the pressure modes.

The information in the tables that present results for plates and cylinders is organized as follows: the first row shows the method or software (SW) used to obtain the results; the second row gives the references; the third row gives the computational time to calculate the wet results; and the fourth and the fifth row give the number of DOF in the finite element model and the DOF in the boundary element mesh, respectively.

The norm of the added mass matrix of the last four columns in Table 2 using FAESOR are 2.1739, 2.5127, 2.7337, and 2.8482, while the norm of the mass matrix is 1 because stiffness and mass matrices were transformed using the dry eigenvectors. We can observe that the values of the added mass matrices' norm increase as the BEM mesh gets coarser. The error of the solutions using interpolation in the last three columns in comparison with the results without interpolation given in the fourth column is given in Table 3.

It is important to notice that the reduction computational time to obtain the results in the first column is 93% with a maximum error of 3.8%.

The results of the modes of vibration for the submerged unconstrained plate are presented in Fig. 2.

Table 1 Dry natural frequencies of an unconstrained plate

Method/SW	Test	ADINA	FAESOR	RITZ
Reference	[19]	[19]	Present	[25]
Time		4×3947		215 s
DOF			12825	1600
Mode	Hz	Hz	Hz	Hz
1	641	645	650	657
2	712	716	719	737
3	1577	1585	1594	1646
4	1766	1766	1779	1821
5	2139	2115	2154	2207

Table 2 Wet natural frequencies of an unconstrained plate

Method/SW	Test	ADINA	FAESOR	FAESOR	FAESOR	FAESOR
Reference	[19]	[19]	Present	Present	Present	Present
Time			42 s	3 s	0.83 s	0.42 s
DOF FEM		4×3947	12,825	12,825	12,825	12,825
DOF BEM			1875	507	243	147
Mode	Hz	Hz	Hz	Hz	Hz	Hz
1	497	489	517	500	496	500
2	575	561	581	560	548	544
3	1293	1277	1318	1279	1272	1289
4	1408	1411	1463	1432	1447	1502
5	1758	1740	1794	1726	1698	1704

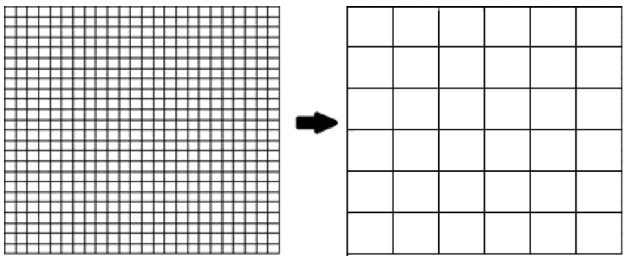

Fig. 1 (Left) 24×24 finite element mesh used to obtain the dry modes and (right) 6×6 coarse boundary element mesh used to compute the pressure modes

3.2 Clamped Square Plate. This example shows the results of the natural frequencies and modes of vibration of a plate in cantilever submerged in water. The plate has dimensions $a = 10$ m and $b = 10$ m along directions x and y, thickness $h = 0.238$ m, while the material properties are Poisson's ratio $\nu = 0.3$, density $\rho_p = 7850\,\text{kg/m}^3$, and Young's modulus $E = 206\,\text{GPa}$. The density of the water is $\rho_w = 1000\,\text{kg/m}^3$.

Table 4 shows experimental results of the natural frequencies of the dry plate presented by Lindholm et al. [20], results using the Rayleigh–Ritz method [25], and results obtained using the commercial FEM code COMSOL [26] and results using H8 elements

Table 3 Error of the wet natural frequencies of an unconstrained plate using interpolation

DOF FEM	12,825	12,825	12,825
DOF BEM	507	243	147
Time reduction (%)	93	98	99
Mode	Error %	Error %	Error %
1	−3.3	−4.1	−3.3
2	−3.6	−5.7	−6.4
3	−3.0	−3.5	−2.2
4	−2.1	−1.1	2.7
5	−3.8	−5.4	−5.0

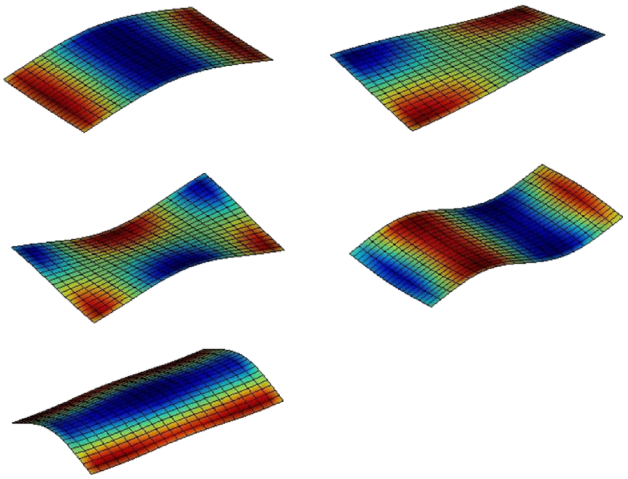

Fig. 2 Modes of vibration of a submerged unconstrained plate. The figures correspond to mode 1 (top-left), mode 2 (top-right), mode 3 (center-left), mode 4 (center-right), and mode 5 (bottom-left).

in FAESOR. The model in FAESOR was built using 40 elements in the x and y directions and seven elements across the thickness.

The results of the natural frequencies of the plate in cantilever submerged in water are presented in Tables 5 and 6. The results obtained in FAESOR are compared to the experimental results presented by Lindholm et al. [20], the numerical results published by Fu and Price [11], and the results obtained using the commercial code COMSOL. The first set of results using the procedure described in this work (FAESOR) corresponds to the model presented in Table 4 with 40×40 elements computing the pressure modes for all elements. The last three columns of Tables 5 and 6 present results computing the pressure modes using coarser boundary element meshes (20×20, 10×10, and 5×5 elements along the length and width of the plate).

It is worth noting that the results of the first five modes of vibration of the cantilever plate obtained in COMSOL with a model having 4030 DOF shown in Tables 5 and 6 correspond to the same modes of vibration obtained with the present approach implemented in FAESOR.

The norm of the added mass matrix of the last four columns in Tables 5 and 6 using FAESOR are 3.2824, 3.7207, 4.4013, and 4.9874.

The modes of vibration obtained with the present approach for the submerged plate are presented in Fig. 3.

3.3 Unconstrained Cylinder: Price and Randall. This example shows the results of the natural frequencies and modes of vibration of an unconstrained cylinder submerged in water presented by Price et al. [21], Randall [22], and Gilroy [23]. The cylinder has the following dimensions: length 1.284 m, diameter 0.357 m, wall thickness 0.003 m, and end cap thickness 0.003 m, while the material properties are Poisson's ratio $\nu = 0.29$, density $\rho_p = 7750\,\text{kg/m}^3$, and Young's modulus $E = 207\,\text{GPa}$. The density of the water is $\rho_w = 1000\,\text{kg/m}^3$.

In this section, the results of the natural frequencies and modes of vibration of the cylinder in vacuo were obtained using the H20 element in the finite element code FAESOR. The finite element model was built using 32, 30, and 1 elements in the circumferential, axial, and radial directions, respectively. The

Table 4 Dry natural frequencies of a clamped plate

Method	Test	RITZ	COMSOL	FAESOR
Reference	[20]	[25]	Present	Present
Time		1600		360 s
DOF			4030	10,080
Mode	rad/s	rad/s	rad/s	rad/s
1	12.30	12.81	12.84	12.74
2	30.78	31.39	31.27	30.87
3	75.46	78.53	78.53	77.77
4	99.84	100.35	99.96	98.98
5	110.57	114.21	113.65	112.18

Table 5 Wet natural frequencies of a clamped plate

Method	Test	Numerical	COMSOL	FAESOR	FAESOR	FAESOR	FAESOR
Reference	[20]	[11]	Present	Present	Present	Present	Present
FEM DOF			149,754	39,360	39,360	39,360	39,360
BEM DOF				5043	1323	363	108
Time				323 s	22.2 s	3.34 s	2.07 s
Mode	rad/s	rad/s	rad/s	rad/s	rad/s	rad/s	rad/s
1	6.56	7.35	7.34	7.18	6.95	6.61	6.20
2	19.66	20.2	20.74	21.06	20.11	18.90	18.03
3	45.32	50.45	49.27	51.74	49.42	46.60	45.46
4	68.18	70.41	69.67	72.01	68.55	65.06	66.75
5	74.69	78.85	78.96	81.01	77.14	73.00	73.14

Table 6 Error of the wet natural frequencies of a cantilever plate using interpolation

Method	FAESOR	FAESOR	FAESOR
Reference	Present	Present	Present
FEM DOF	39,360	39,360	39,360
BEM DOF	1323	363	108
Time reduction (%)	93	98.9	99.4
Mode	%	%	%
1	−3.2	−7.9	−13.6
2	−4.5	−10.3	−14.4
3	−4.5	−9.9	−12.1
4	−4.8	−9.7	−7.3
5	−4.8	−9.9	−9.7

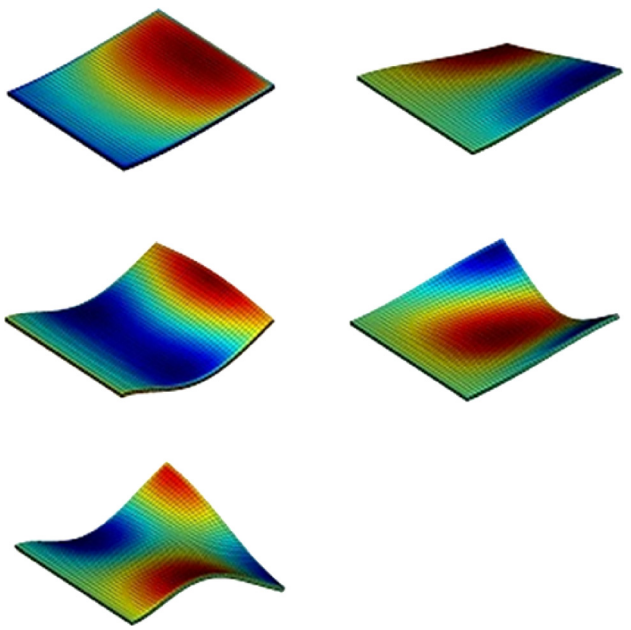

Fig. 3 Modes of vibration of a submerged cantilever plate. The figures correspond to mode 1 (top-left), mode 2 (top-right), mode 3 (center-left), mode 4 (center-right), and mode 5 (bottom-left).

boundary element mesh is built on the exterior surface of the cylinder, where each square surface of the finite element mesh is represented by two triangular boundary elements.

Sections 3.3 and 3.4 including cylinders show that this method can be applied in an easier way to any geometry with smooth changes in its geometry. Geometries with drastic changes, such as closed cylinders presented in this work, have to be solved more carefully. For each of the cylinders in this work, it is possible to see that the three surfaces of the BEM mesh, cylindrical part and two circular plates, vibrate with discontinuities along the edges of the cylinder. Thus, the added mass must be computed individually for each part without taking into account the modes of vibration of the other two parts.

Table 7 shows the results of the dry frequencies obtained experimentally and using the FEM code NASTRAN presented by Price et al. [21], by Gilroy [23] using the finite element (FE) code VAST, results obtained using the FEM code ABAQUS using 294 S8R elements and results using FAESOR. The modes in Tables 7–9 are classified as (m, n), where m is the axial wave number and n is the circumferential wave number. End plate modes in Tables 7–9 are identified as e1 and e2.

Table 8 shows the results of the wet modes of the cylinder. The results obtained with the present approach (FAESOR) are compared again with the results given by Price et al. [21] and Gilroy [23]. The first set of results using FAESOR corresponds to the solution computing the pressure modes on the fine mesh, where the location of the triangular boundary elements is defined by the external surfaces of the FEM mesh. The second set of results using FAESOR was computed using a boundary element mesh discretizing the cylinder in 16, 30, and 1 elements in the circumferential, axial, and radial directions, respectively, and linear interpolation was used to compute the pressure modes at the location of the surface nodes of the FEM mesh. The computed wet modes are shown in Fig. 4. The set of results using interpolation did not give the same eigenvalues for pairs corresponding to the same mode. For this reason, both results are included in Table 8. Good approximations of the frequencies were obtained for modes (1, 2) and (1, 3). This may indicate that for higher modes, finer meshes of the BEM are needed to obtain more accurate results. This is because the change in the BEM is too coarse to have a good representation of the modes of vibration and pressure modes cannot be computed with enough accuracy. Similarly, the end cap modes were obtained from a very coarse BEM mesh which explains why the error is higher than for modes (1, 2) and (1, 3).

Norm of the added mass matrices of the last two columns in Table 8 are 15.2342 and 21.6817.

3.4 Unconstrained Cylinder: Everstine and Gilroy. This example shows the results of the natural frequencies and modes of vibration of an unconstrained cylinder submerged in water presented by Everstine [10] and Gilroy [23]. The cylinder has the following dimensions: length 60 m, diameter 10 m, wall thickness 0.05 m, and endcap thickness 0.003 m, while the material properties are Poisson's ratio $\nu = 0.3$, density $\rho_p = 7900\,\text{kg/m}^3$, and Young's modulus $E = 196\,\text{GPa}$. The density of the water is $\rho_w = 1000\,\text{kg/m}^3$.

In this section, the same procedure as in Sec. 3.3 was used to compute the results using FAESOR. Table 10 shows the results of the dry frequencies presented by Everstine [10] using the FEM code NASTRAN, by Gilroy [23] using the finite element code VAST, results obtained using 294 S8R elements in the FEM code ABAQUS [27] and results using FAESOR.

The results of the natural frequencies and wet modes are shown in Tables 11 and 12.

3.5 Unconstrained Ear-Bone. This example shows the results of the natural frequencies of an unconstrained ear-bone of approximately $2.5\,\text{cm}^3$. The material properties of the bone are Poisson's ratio $\nu = 0.25$, density $\rho_{\text{bone}} = 2500\,\text{kg/m}^3$, and Young's modulus $E = 20\,\text{GPa}$. The density of the water is $\rho_w = 1000\,\text{kg/m}^3$.

Figure 5 shows the finite element and boundary element meshes. The results of the natural frequencies in dry and wet conditions are shown in Table 13. Two different finite element meshes were used to calculate the dry natural frequencies with 387552 and 320706 tetrahedra, respectively. Some volumes of thin bone increased thickness during the meshing process which led to somewhat higher natural frequencies. Three results are given for the wet natural frequencies. The first two sets of results correspond to the models presented for the dry solution with a fine mesh and a coarse mesh, respectively. The third set of results corresponds to the solution using the fine finite element mesh with its corresponding boundary element mesh. The fourth set of results shows the wet frequencies obtained using the fine finite element mesh but using the boundary element mesh corresponding to the coarse mesh. Finally, the fifth column presents the results obtained using the coarse finite element mesh and the coarse boundary

Table 7 Dry natural frequencies of an unconstrained cylinder

Method	Test	FE	VAST FE8	VAST FE4	ABAQUS	FAESOR
Reference	[21]	[21]	[23]	[23]	Present	Present
Time						5122 s
FEM DOF						524,288
Mode (m, n)	Hz	Hz	Hz	Hz	Hz	Hz
(1,2)	194	198	196	202	197	196
(1,3)	198	204	199	208	203	208
(e1)	—	209	220	235	223	237
(e2)	—	217	228	240	232	245
(1,4)	336	354	341	367	359	365
(2,3)	387	404	388	439	399	391
(2,4)	403		405	439	440	425
(3,4)	565		570	655	638	584

Table 8 Wet natural frequencies of an unconstrained cylinder

Method	Test	FE	Anal.	VAST	FAESOR	FAESOR
Reference	[21]	[21]	[23]	[23]	Present	Present
Time					551 s	139 s
FEM DOF					524,288	524,288
BEM DOF					16,146	6066
Mode (m, n)	Hz	Hz	Hz	Hz	Hz	Hz
(1,2)	96	98	106	90.5	96	93.6/96.0
(1,3)	107	109	123	115	105	108/110
(e1)	—	—	91.8	85.3	88.9	78.8
(e2)	—	—	101	85.3	112	103
(1,4)	199	204	253	238	190	207/207
(2,3)	214	215	266	266	198	209/209
(2,4)	239	241	—	301	222	229/245
(3,4)	341	340	—	—	308	341/375

Table 9 Error of the wet natural frequencies of an unconstrained cylinder using interpolation

Method	FAESOR
Reference	Present
Time	139 s
FEM DOF	524,288
BEM DOF	6066
Mode (m, n)	Hz
(1,2)	−2.5/0
(1,3)	2.9/4.8
(e1)	−11.4
(e2)	−8
(1,4)	8.9
(2,3)	5.6/5.6
(2,4)	3.2/10.4

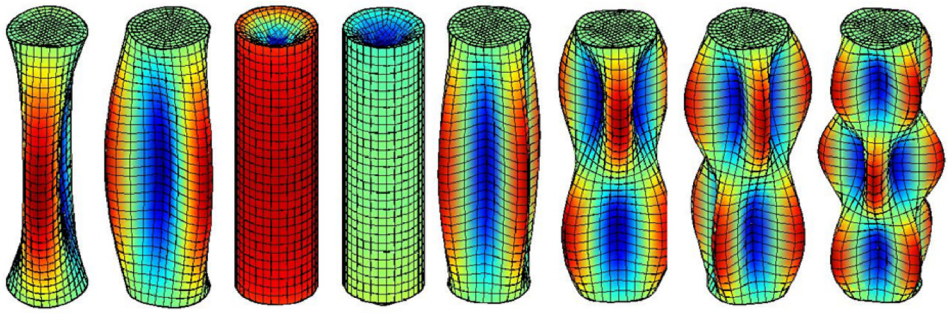

Fig. 4 Modes of vibration of the unconstrained cylinder presented by Price. Modes correspond in order to the modes presented in Table 7, from left to right (1,2), (1,3), (e1), (e2), (1,4), (2,3), (2,4), and (3,4). Plate modes have a zero pressure along the cylinder.

Table 10 Dry natural frequencies of an unconstrained cylinder

Method	FEM	VAST 8 FE4	ABAQUS	FAESOR
Reference	[10]	[23]	Present	Present
Time				5122 s
FEM DOF				524,288
Mode (n, m)	Hz	Hz	Hz	Hz
(1,2)	2.72	2.72	2.72	2.72
(1,3)	3.90	3.85	3.91	3.95
(e1)	4.22	4.88	5.01	4.99
(e2)	—	—	5.22	5.11
(2,3)	—	—	5.96	5.86
(1,4)	7.19	7.08	7.38	7.36
(2,4)	—	—	8.08	7.86

element mesh. Obviously, the dry solution of the finer finite element model is more accurate than the solution of the coarser mesh. Similarly, the wet results using the finer finite element mesh and finer boundary element mesh are more accurate than the other solutions.

Norm of the added mass matrices of the last two columns in Table 13 are 6.3565, 7.8752, and 9.4289.

Another observation from Table 13 is that when the error of the results using a coarse mesh is obtained comparing the results by those obtained using a fine mesh, dry natural frequencies have a larger error than the wet natural frequencies. The fourth set of results in Table 13 was obtained using the finer finite element mesh and the coarser boundary element mesh. This last set of results deviates a maximum of 2.02% in comparison with the results using the finer boundary element mesh, but the computational cost was only 5.5 h instead of 42.5 h.

Table 11 Wet natural frequencies of an unconstrained cylinder

Method	Test	FEM	FAESOR	FAESOR
Reference	[10]	[23]	Present	Present
Time			551 s	139 s
FEM DOF			524,288	524,288
BEM DOF			16,146	6066
Mode (n, m)	Hz	Hz	Hz	Hz
(1,2)	1.13	1.25	1.04	0.96/1.00
(1,3)	1.81	2.06	1.55	1.54/1.57
(e1)	1.44	2.01	1.51	1.32
(e2)	—	—	1.88	1.71
(1,4)	3.67	4.45	2.99	3.15/3.38
(2,3)	—	—	2.31	2.32/2.36
(2,4)	—	—	3.21	3.60/3.85

Table 12 Error of the wet natural frequencies of an unconstrained cylinder using interpolation

Method	FAESOR
Reference	Present
Time	139 s
FEM DOF	524,288
BEM DOF	6066
Mode (n, m)	Hz
(1,2)	−7.7/−3.8
(1,3)	−0.6/1.3
(e1)	−12.6
(e2)	−9.0
(1,4)	5.4/13.0
(2,3)	0.4/2.2
(2,4)	12.1/19.9

4 Conclusions

The present approach to calculate the natural frequencies of submerged structures uses a fine mesh in the FEM to solve for the natural frequencies and modes of vibration of the structure in vacuo, and then, an added mass matrix obtained through the use of a coarse mesh in the BEM is used to solve for the natural frequencies of the submerged structure. The use of the coarse mesh in the BEM considerably reduced the computational cost of the computations of natural frequencies of structures in contact with inviscid fluid with small variations in the results. For instance, when solving for the natural frequencies of the submerged ear bone presented in Sec. 3.5, the results using a coarse boundary element mesh required only 13% of the computational cost needed to carry out the same computation using a fine boundary element mesh, while the difference between the first five wet natural frequencies was kept within 2.02%. The reduction in the present approach is achieved interpolating the values of the pressure modes at the nodes of a coarse boundary element mesh to the nodes on a finer boundary element mesh. This (a) avoids the large number of numerical integrations in the BEM, as well as (b) reduces the cost of solving systems of coupled linear algebraic equations with large dense matrices whose computational cost scales as number of unknowns cubed, i.e., very poorly. Other key points in this work are (a) the definition of appropriate numerical integrations schemes to solve the singular integrals characteristic of the BEM over quadrilateral and triangular elements and (b) surfaces of structures with angles close to 90 deg must be split prior to interpolation, as these surfaces may not move or move in different directions than the contiguous-normal surfaces in specific modes of vibration, and thus, interpolation must be carried out between nodes belonging to the same surface only.

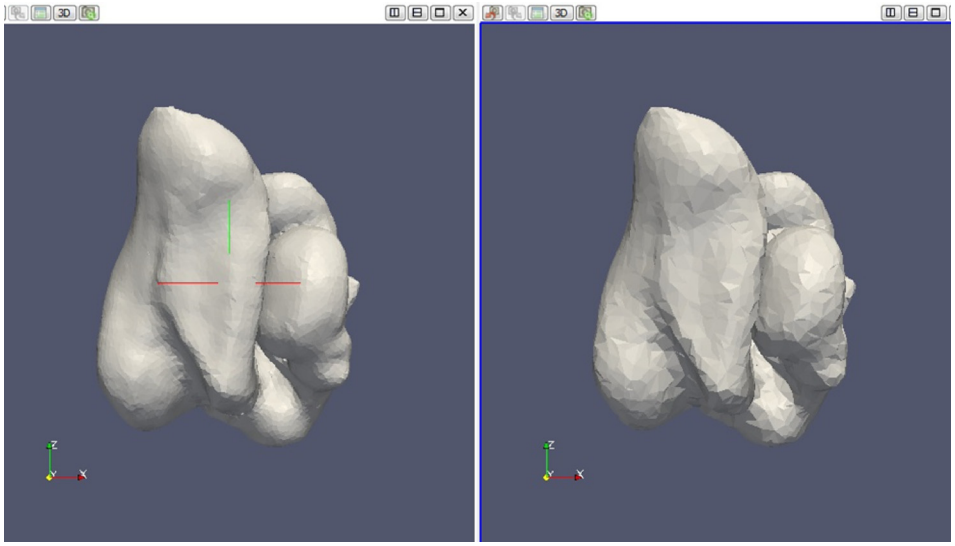

Fig. 5 (Right) finite element mesh used to obtain the dry modes and (left) coarse boundary element mesh used to compute the pressure modes of the ear-bone

Table 13 Dry and wet natural frequencies of an unconstrained ear-bone

Condition	Dry	Dry	Wet	Wet	Wet
Method	FAESOR	FAESOR	FAESOR	FAESOR	FAESOR
Time	387,552		42.5 h	5.5 h	5.5 h
Finite elem		320,706	387,552	387,552	320,706
BEM DOF			52,170	18,732	18,732
Mode (n, m)	kHz	kHz	kHz	kHz	kHz
1	12.910	14.736	10.059	9.929	10.826
2	16.996	19.426	14.360	14.185	15.573
3	24.036	26.470	19.778	19.434	20.653
4	30.292	33.862	25.636	25.238	27.053
5	39.097	42.236	30.953	30.326	31.378

Nomenclature

$\mathbf{a}$ = vector of unknown coefficients
a, b = plate dimensions (width and length)
A_{ij} = coefficient matrix in the boundary element method
B_{ij} = coefficient matrix in the boundary element method
$\mathbf{c}$ = vector of unknown coefficients
D = surface of the structure
E = Young's modulus
E_i = the ith boundary element
f = basis vectors of the fluid pressure also called pressure modes
G = free-space Green's function in three dimensions for the Laplace equation
h = plate thickness
i, j = subscripts
$\mathbf{I}$ = identity matrix
$\mathbf{J}$ = Jacobian
$\mathbf{K}$ = stiffness matrix
$\mathbf{M}$ = mass matrix
m_{ii} = terms of the diagonal mass matrix
m_{ij}^* = terms of the added mass terms
$\mathbf{M}^*$ = added mass matrix
$\mathbf{n}$ = unit normal toward the exterior of the solid domain
N = number of flat boundary elements
P = modal amplitude of the fluid pressure
PV = principal-value integral
$r = r = |\mathbf{x} - \mathbf{x}_0|$
S = surface of the structure
$\mathbf{U}$ = modal amplitude of the structural displacements
w = weight in numerical integrations
x, y = directions
$\mathbf{x}$ = vector defining the location of the variable "field point"
$\mathbf{x}_j^M$ = centroid of jth boundary element
$\mathbf{x}_0$ = fixed location of the "singular point"
δ_{ij} = Kronecker's delta
$\partial p/\partial n$ = normal derivative of the pressure
∇ = nabla operator
π = ratio of a circle's circumference to its diameter
ρ_{bone} = density of the bone
ρ_{F} = density of the fluid
ρ_p = density of the plate or structure
ρ_w = density of water
ν = Poisson's ratio
$\mathbf{\Psi}$ = modal matrix in which columns $\boldsymbol{\psi}_i$ are the corresponding ith orthogonal eigenvectors that define the modes of vibration
ω = circular frequency
Ω^2 = diagonal matrix containing the eigenvalues of the generalized eigenvalue problem
$\mathbf{0}$ = null vector

References

[1] Lin, Z., and Liao, S., 2011, "Calculation of Added Mass Coefficients of 3D Complicated Underwater Bodies by FMBEM," Commun. Nonlinear Sci. Numer. Simul., **16**(1), pp. 187–194.
[2] Ghassemi, H., and Yari, E., 2011, "The Added Mass Coefficient Computation of Sphere, Ellipsoid and Marine Propellers Using Boundary Element Method," Pol. Maritime Res., **68**(1), pp. 17–26.
[3] Geers, T. L., 1978, "Doubly Asymptotic Approximations for Transient Motions of Submerged Structures," J. Acoust. Soc. Am., **64**(5), pp. 1500–1508.
[4] Deruntz, J. A., and Geers, T. L., 1978, "Added Mass Computation by the Boundary Integral Method," Int. J. Numer. Methods Eng., **12**(3), pp. 531–48.
[5] Antoniadis, I., and Kanarachos, A., 1987, "Decoupling Procedure for the Modal Analysis of Structures in Contact With Incompressible Fluids," Commun. Appl. Numer. Methods, **3**(6), pp. 507–517.
[6] Sandberg, G., 1995, "A New Strategy for Solving Fluid-Structure Problems," Int. J. Numer. Methods Eng., **38**(3), pp. 357–370.
[7] Ugurlu, B., and Ergin, A., 2006, "A Hidroelasticity Method for Vibrating Structures Containing and/or Submerged in Flowing Water," J. Sound Vib., **290**(3–5), pp. 572–596.
[8] Rajasankar, J., Iyer, N. R., and Rao, V. S. R. A., 1993, "A New 3-D Finite Element Model to Evaluate Added Mass for Analysis of Fluid-Structure Interaction Problems," Int. J. Numer. Methods Eng., **36**(6), pp. 997–1012.
[9] Kwak, M. K., 1996, "Hydroelastic Vibration of Rectangular Plates," ASME J. Appl. Mech., **63**(1), pp. 110–115.
[10] Everstine, G. C., 1991, "Prediction of Low Frequency Vibrational Frequencies of Submerged Structures," ASME J. Vib. Acoust., **113**(2), pp. 187–191.

[11] Fu, Y., and Price, W. G., 1987, "Interactions Between a Partially or Totally Immersed Vibrating Cantilever Plate and the Surrounding Fluid," J. Sound Vib., **118**(3), pp. 495–513.
[12] Wilken, M., Of, G., Cabos, C., and Steinbach, O., 2009, "Efficient Calculation of the Effect of Water on Ship Vibration," *Analysis and Design of Marine Structures*, S. Guedes and P. K. Das, eds., Taylor & Francis, London, pp. 93–101.
[13] Jensen, F. B., Kupperman, W. A., Porter, M. B., and Schmidt, H., 1994, *Computational Ocean Acoustics*, American Institute of Physics, New York.
[14] Monterrubio, L. E., and Krysl, P., 2012, "Efficient Calculation of the Added Mass Matrix for Vibration Analysis of Submerged Structures," 11th International Conference on Computational Structures Technology, Stirlingshire, UK, Sept. 4–7, Paper No. 212 2012.
[15] Pozrikidis, C., 2002, *A Practical Guide to Boundary Element Methods With the Software Library BEMLIB*, Chapman & Hall/CRC Press, Boca Raton, FL.
[16] Pozrikidis, C., 1998, *Numerical Computation in Engineering and Science*, Oxford University Press, New York.
[17] Pina, H. L. G., Fernandes, J. L. M., and Brebbia, C. A., 1981, "Some Numerical Integration Formulae Over Triangles and Squares With a 1/r Singularity," Appl. Math. Modell., **5**(3), pp. 209–11.
[18] Bathe, K. J., 1982, *Finite Element Procedures in Engineering Analysis*, Prentice Hall, Englewood Cliffs, NJ.
[19] Sundqvist, J., 1983, "An Application of ADINA to the Solution of Fluid-Structure Interaction Problems," Comput. Struct., **17**(5–6), pp. 793–807.
[20] Lindholm, U. S., Kana, D. D., Chu, W. H., and Abramson, H. N., 1965, "Elastic Vibration Characteristics of Cantilever Plates in Water," J. Ship Res., **9**, pp. 11–22.
[21] Price, W. G., Randall, R., and Temarel, P., 1988, "Fluid-Structure Interaction of Submerged Shells," Naval Architecture and Offshore Engineering Conference, Guildford, Surrey, UK.
[22] Randall, R. J., 1990, "Fluid-Structure Interaction of Submerged Shells," Ph.D. dissertation, Brunel University, London.
[23] Gilroy, L. E., 1993, "Finite Element Calculations of Cylinder Natural Frequencies," Defense Research Establishment Atlantic, Ottawa, ON, Canada, Technical Communication No. 93.
[24] Krysl, P., 2012, "FAESOR: Matlab Toolkit for Finite Element Analysis (Computer Software)," San Diego, CA, accessed July 25, 2018, http://hogwarts.ucsd.edu/~pkrysl/faesor
[25] Monterrubio, L. E., and Ilanko, S., 2012, "Sets of Admissible Functions for the Rayleigh-Ritz Method," 11th International Conference on Computational Structures Technology, Stirlingshire, UK, Sept. 4–7, Paper No. 97 2012.
[26] COMSOL, 2009, *Acoustics Module User Guide*, COMSOL, Inc., Burlington, MA.
[27] ABAQUS, 2011, "ABAQUS Version 6.11-2 User's Manual," Simulia, Providence, RI.